Impact of an Electric Truck Charging Station on the Small-Signal Stability of MV Grid

1st Guy Wanlongo Ndiwulu
iMMC - MEED
Université catholique de Louvain (UCLouvain)
Louvain-la-Neuve, Belgium
guy.wanlongo@uclouvain.be

2nd Emmanuel De Jaeger
iMMC - MEED
Université catholique de Louvain (UCLouvain)
Louvain-la-Neuve, Belgium
emmanuel.dejaeger@uclouvain.be

2026 International Conference on Smart Energy Systems and Technologies (SEST) | 979-8-3315-5529-0/26/$31.00 ©2026 IEEE | DOI: 10.1109/SEST67798.2026.11712551

***Abstract*—This paper investigates the impact of an ETCS on the small-signal stability of the medium-voltage (MV) grid to which it is connected. An analytical approach based on a state-space model of the grid that integrates the ETCS is developed to analyze the movement of eigenvalues in the complex plane. In addition, time-domain simulations are conducted to investigate rapid voltage changes and the dynamic response of the power exchanged between the AC grid and the ETCS. The considered DC microgrid is represented by an equivalent model, where the overall system dynamics are dictated by the DC bus. A Belgian local MV network is used as a case study, with dynamic modeling performed in DIgSILENT PowerFactory. The obtained results show that the equivalent truck charger introduces an additional stable mode, whose movement is dictated by the connection rate of the subscribed load power at the load buses. Furthermore, the rapid voltage change resulting from the sequential connection of trucks rated is estimated to be 3.5%**

***Index Terms*—Heavy-duty electric vehicle, EV Charging station, Small-signal stability, Rapid voltage change.**

I. Introduction

The electric truck charging station (ETCS) is regarded as one of the major challenges in the transportation sector, primarily because of the high charging power these vehicles require and the resulting impact on the electrical grid [1]. Compared to the light-duty electric vehicle charging stations, The ETCSs can reach the order of several megawatts or more [2]. This level of power demand may require connecting an ETCS to the medium-voltage (MV) distribution grid. The AC grid can face limitations in host capacity to integrate these charging loads. The incorporation of local generation and energy storage systems within ETCSs can be envisaged as an effective means of mitigating the challenges associated with connecting ETCS to distribution grids with limited hosting capacity [1]–[4]. Under these conditions, the ETCS can be regarded as a microgrid. The connection of a microgrid-based ETCS to the public grid may be perceived by the grid as an active load interfaced through a power-electronic converter. Such an AC-grid connection can introduce grid dynamic and power quality issues, including small-signal stability concerns.

Most studies in the literature focus on the dynamic impacts of light-duty electric vehicle charging stations on power grids, including hosting-capacity limitations and associated mitigation strategies [1], [5]–[9]. In contrast, only a limited number of studies have examined the impact of ETCSs on small-signal stability of the public grid is rarely addressed [5], [7]. Reference [5] investigates the impact of medium- and heavy-duty electric vehicle charging stations on a benchmark IEEE 33-bus distribution system stability. However, the authors focus their analysis on the voltage profile of the AC grid, without addressing grid dynamic impacts related to small-signal stability or rapid voltage changes. In [14], the authors analyze the grid impact of large-scale heavy-duty charging infrastructure. Their study focuses on transformer loading, line utilization, and voltage profiles by comparing scenarios with and without an ETCS; however, grid dynamic issues are not addressed. Reference [15] investigates the impacts of depot charging on distribution grids under various charging strategies, the analysis is limited to assessing the effects on the voltage profile of the distribution feeder.

This paper investigates the effects of an ETCS on the small-signal stability and rapid voltage changes of a MV grid, using a Belgian local MV network as a case study. Analytical state-space models are developed for the equivalent ETCS and the MV feeder. The caused grid dynamic impacts on small-signal stability are assessed by analyzing the trajectories of the system modes in the complex plane. In addition, time-domain simulations are conducted to analyze rapid voltage changes at the point of common coupling (PCC).

The remainder of this paper is organized as follows. Section II describes the modeling of the MV grid integrating the ETCS. Section III presents the proposed state-space models of the feeder and the ETCS, while Section IV provides the small-signal stability results. Finally, Section V concludes the paper.

II. Local medium-voltage grid model

A. Local MV grid architecture model

Fig. 1 illustrates the architecture of the local MV grid integrating an ETCS at the point of common coupling (PCC). The ETCS is connected to the AC grid through a 10 kV/0.4 kV transformer. The MV grid is connected to the 70 kV network through the TS transformer station 70 kV/10 kV. The high-voltage grid is characterized by an estimated short-circuit capacity of 803 MVA. It is linked to the MV level via the transformers with a combined capacity of 100 MVA. This MV network operates at a voltage level of 10 kV. It consists of 17 nodes and two half-loops.

Authorized licensed use limited to: Univ Catholique de Louvain/UCL. Downloaded on November 10,2026 at 18:00:57 UTC from IEEE Xplore. Restrictions apply.

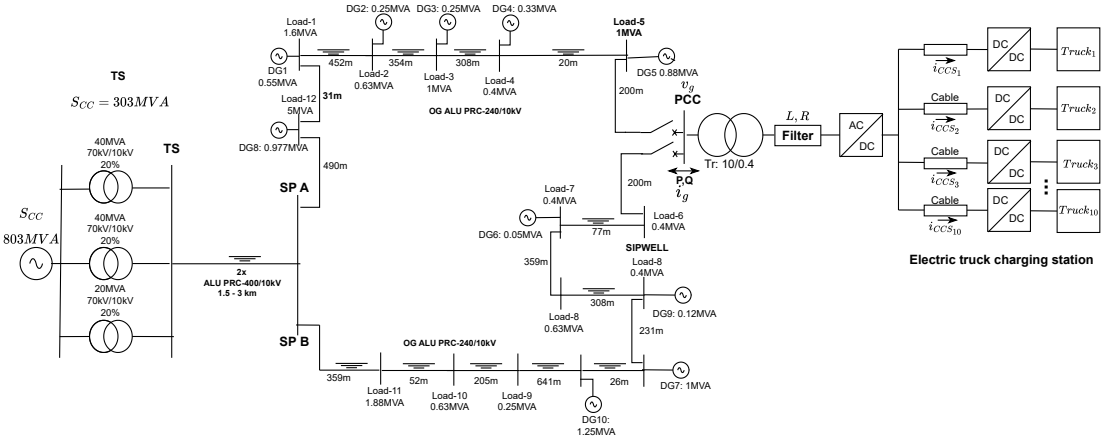


Fig. 1. Local medium-voltage grid with an integrated DC-microgrid-based electric truck charging station.

B. Distributed generator models

Since no information is available on the types of DGs connected to this grid, we assume that all local DGs are inverter-based resources (IBRs). These DGs are represented by generic models of the active (P) and reactive (Q) power control structures, as well as the converter. Fig. 2 illustrates the generic model proposed in the literature [10]. This model comprises three submodels: the plant-level control model, the electrical control model, and the converter model. It is a generic model applicable to photovoltaic systems and Type 4 wind turbines.

The dynamic modeling approach proposed in this paper incorporates both the electrical and converter models. The

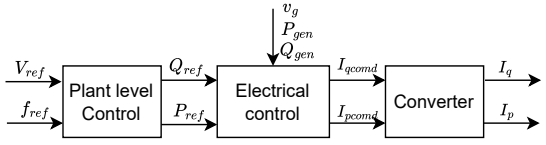


Fig. 2. Generic model of inverter-based resources for WECC.

generic model of a PQ control structure comprises an active power control loop, a reactive power control loop, and a voltage control loop. Active and reactive power are regulated through the active current (i_p) and reactive current (i_q), respectively. The setpoint of reactive power is determined on the basis of the specified power factor. The voltage is regulated using the droop control, with the output of the voltage droop controller added to the reactive current signal. In contrast, the generic generator converter model comprises a high-voltage reactive current control block and a low-voltage active current control block. The first part is associated with the reactive current component and the grid voltage, while the second part relates to the active current.

C. Dynamic model of electric truck charging station

A common unipolar DC-bus architecture is considered, as described in Fig. 1. The system includes a front-end active rectifier that interfaces the AC grid with the charging station (CS), as illustrated in Fig. 1. Each charger consists of a buck converter that steps down the DC voltage from 750 V to the 500 V required by the electric truck.

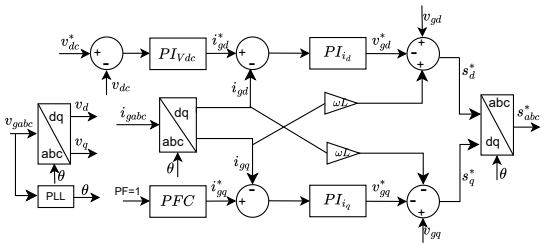


Fig. 3. Control structure of the front-end rectifier.

1) EV charger modelling and control: The complete dynamic model of the charger is obtained by combining individual dynamic models of front-end actice rectifier, a step-down (buck) converter, and an integrated energy-storage unit representing the off-board battery system of the electric truck.

- Dynamic model of the front-end active rectifier

This dynamic model is derived from the average model of the three-phase rectifier.As illustrated in Fig. 1, the dynamic model of this rectifier can be described by the following equations:

$$v_{gd} = L\frac{di_{gd}}{dt} + Ri_{gd} - \omega Li_{gq} + S_d v_{dc} \tag{1}$$

$$v_{gq} = L\frac{di_{gq}}{dt} + Ri_{gq} + \omega Li_{gd} + S_q v_{dc} \tag{2}$$

$$i_{dc} = C_{dc}\frac{dv_{dc}}{dt} + i_{load} \tag{3}$$

where v_{gd} and v_{gq} are the direct and quadrature components of the grid voltage, respectively. i_{gd} and i_{gq} denote the direct and quadrature components of the current drawn by the ETCS. ω is the frequency associated with the synchronous rotation of the $dq-$axis reference frame. S_d and S_q denote the direct and quadrature components of the IGBT switching states.

Fig. 3 presents a decoupled regulation of the DC output voltage and reactive power. The DC voltage is managed through an outer voltage control loop combined with an inner current control loop. Reactive power is regulated via the quadrature (q-axis) component of the current. To facilitate control in

Authorized licensed use limited to: Univ Catholique de Louvain/UCL. Downloaded on November 10,2026 at 18:00:57 UTC from IEEE Xplore. Restrictions apply.

the rotating $dq-$axis synchronous reference frame, a Phase-Locked Loop (PLL) is employed to generate the instantaneous angle.

- Dynamic model of the DC-DC converter

The dynamic model for the step-down converter can be derived as follows.

$$V_{dc} = V_B + L\frac{di_{load}}{dt} \tag{4}$$

$$i_{load} = i_B + C_B\frac{dV_B}{dt} \tag{5}$$

where L and C_B denote the inductance and capacitance of the step-down converter, respectively. i_B and V_B are the current and voltage of the truck battery. The battery is modeled as a variable voltage source in series with an internal resistance and a parallel capacitance, as described in [11].

As illustrated in [12], two equivalent control strategies of the step-down converter—constant current and constant voltage—can be implemented depending on the desired regulation strategy.

- Active power consumption of the ETCS, and voltage magnitude at the PCC

The ETCS is assumed to operate at a unity power factor; therefore, the quadrature component of the current in the rectifier control is zero ($i_{gq} = 0$), the active power P_{CS} consumed by the ETCS is described by the following equations:

$$P_{CS} = \frac{2R}{3S_d^2}\left(C_{dc}\frac{dV_{dc}}{dt} + \sum_{i=1}^{10}\left(i_{B_i} + C_{B_i}\frac{dV_{B_i}}{dt}\right)\right)^2 + V_{dc}C_{dc}\frac{dV_{dc}}{dt} + V_{dc}\sum_{i=1}^{10}\left(i_{B_i} + C_{B_i}\frac{dV_{B_i}}{dt}\right) \tag{6}$$

Under steady-state conditions, this power comprises two distinct components: a constant impedance load , defined by its equivalent impedance as seen from the DC side of the rectifier- and a constant power load, representing the power drawn by the truck via the DC-DC converter.

The voltage at the PCC is given by the following equation:

$$V_{PCC} = 0.707\sqrt{A \pm \sqrt{B} - C} \tag{7}$$

with $A = V_g^2 - 2P_{CS}R - 2Q_{CS}X$, $C = 4(P_{CS}^2 + Q_{CS}^2(R^2 + X^2)$ and $B = \sqrt{(V_g^2 - 2P_{CS}R - 2Q_{CS}X)^2}$

Equation (7) indicates that the voltage at the PCC depends on the power exchanged between the ETCS and the AC grid, as well as on the electrical characteristics of the AC grid.

III. Small-signal stability model

A. State-space model of distributed generators

The power and current control structures associated with the electrical model and the converter model, as described in [10], are shown in Fig. 4. The signals at the outputs of the filters and controllers are treated as dynamic signals that dictate the dynamic behavior of inverter-based resources.

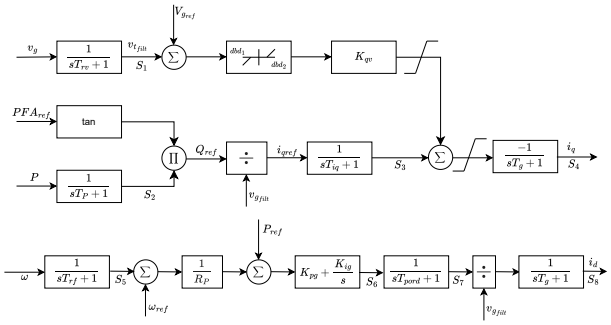


Fig. 4. Generic model integrating PQ control and converter dynamics for regulating active and reactive power injection by DGs into the grid.

The differential equations governing each i^{th} inverter-based resource connected to the grid are given by:

$$\frac{ds_{1_i}}{dt} = \frac{1}{T_{ref_i}}(v_{g_i} - s_{1_i}) \tag{8}$$

$$\frac{ds_{2_i}}{dt} = \frac{1}{T_{P_i}}(P_i - s_{2_i}) \tag{9}$$

$$\frac{ds_{3_i}}{dt} = \frac{1}{T_{iq_i}}\left(s_{2_i}\frac{tan(PFA_i)}{v_{g_{0_i}}} - s_{3_i}\right) \tag{10}$$

$$\frac{ds_{4_i}}{dt} = \frac{1}{T_{g_i}}\left(-V_{g_{ref_i}}K_{qv_i} - s_{1_i}K_{qv_i} - s_{3_i} - s_{4_i}\right) \tag{11}$$

$$\frac{ds_{5_i}}{dt} = \frac{1}{T_{rf_i}}(\omega_i - s_{5_i}) \tag{12}$$

$$\frac{ds_{6_i}}{dt} = \left(\frac{K_{ig_i}}{R_{P_i}} - \frac{K_{pg_i}}{R_{P_i}T_{rf_i}}\right)s_{5_i} + \frac{K_{pg_i}}{R_{P_i}T_{rf_i}}\omega_i - \frac{K_{ig_i}}{R_{P_i}}\omega_{ref_i} + K_{ig_i}P_{ref_i} \tag{13}$$

$$\frac{ds_{7_i}}{dt} = \frac{1}{T_{pord_i}}(s_{6_i} - s_{7_i}) \tag{14}$$

$$\frac{ds_{8_i}}{dt} = \frac{1}{T_{g_i}}\left(\frac{s_{7_i}}{v_{g_i}} - s_{8_i}\right) \tag{15}$$

$$v_{gd_i} - R_i i_{gd_i} + \omega L_i i_{gq_i} - V_{g_i}\ sin(\delta_i - \theta_i) = 0 \tag{16}$$

$$v_{gq_i} - R_i i_{gq_i} - \omega L_i i_{gd_i} - V_{g_i}\ cos(\delta_i - \theta_i) = 0 \tag{17}$$

where S_{1_i} denotes the voltage signal at the output of the voltage filter. S_{2_i} represents the active power signal at the output of the power filter. S_{3_i} is the reactive current at the output of the current filter. S_{4_i} indicates the reactive current supplied by the converter. S_{5_i} is the frequency signal at the output of the frequency filter. S_{6_i} represents active power signal at the output of the proportional-integral controller. S_{7_i} is the active power signal at the output of the power filter. S_{8_i} indicates the active current supplied by the converter. T_{p_i} and T_{rf_i} are the transducer time constants for power and frequency measurements, respectively. T_{iq} is the Q control time constant. K_{qv_i} denotes proportional voltage control gain.

Authorized licensed use limited to: Univ Catholique de Louvain/UCL. Downloaded on November 10,2026 at 18:00:57 UTC from IEEE Xplore. Restrictions apply.

K_{ig_i} and K_{pg_i} represent the integral and proportional gains of the active-power controller. T_{g_i} is the current control time constant. T_{pord_i} denotes power order time constant. PFA_i is the power-factor angle. R_{p_i} is the frequency control droop.

By linearizing (8)–(17) around an operating point, and by neglecting the terms of second and higher order of small perturbations (Δi) and input vector in the Taylor-series expansion, the state-space model of DGs can be expressed as follows:

$$\Delta\dot{X} = A_{IBR}\Delta X + B_{IBR1}\Delta U_1 + B_{IBR2}\Delta U_2 \tag{18}$$

$$0 = C_{IBR}\Delta X + D_{IBR1}\Delta I_g + D_{IBR2}\Delta V_g \tag{19}$$

where $\Delta X = [\Delta X_1\ \Delta X_2\ \dots\ \Delta X_{10}]^T$ represents the state vector composed of the state subvector of each inverter-based resource (IBR) connected to the AC grid. They are defined by $\Delta X_i = [\Delta s_1\ \Delta s_2\ \Delta s_3\ \Delta s_4\ \Delta s_5\ \Delta s_6\ \Delta s_7\ \Delta s_8]^T$. $\Delta U_1 = [\Delta v_{g_i}\ \Delta\omega_i\ \Delta P_i]^T$, and $\Delta U_2 = \left[\Delta v_{g_{ref_i}}\ \Delta\omega_{ref_i}\ \Delta P_{ref_i}\right]^T$ are the input matrices of IBRs. Δv_{g_i}, ω_i and ΔP_i denote the small-signal variations of the AC grid voltage, grid frequency, and active power, respectively. Their corresponding small-signal reference values are denoted by $\Delta v_{g_{ref_i}}$, ω_{ref_i} and ΔP_{ref_i}.

Matrices A_{IBR}, B_{IBR1}, B_{IBR2}, C_{IBR}, and D_{IBR} are expressed as:

$$A_{IBR} = \begin{bmatrix} A_{IBR_1} & 0 & \dots & 0 \\ 0 & A_{IBR_2} & \dots & 0 \\ \vdots & \vdots & \ddots & \vdots \\ 0 & 0 & \dots & A_{IBR_{10}} \end{bmatrix}_{80\times80};$$

$$A_{IBR_i} = \begin{bmatrix} A_{IBR_{1i}} & A_{IBR_{2i}} \\ A_{IBR_{3i}} & A_{IBR_{4i}} \end{bmatrix}_{8\times8};$$

$$A_{IBR_{1i}} = \begin{bmatrix} \frac{-1}{T_{rf_i}} & 0 & 0 & 0 \\ 0 & \frac{-1}{T_{P_i}} & 0 & 0 \\ 0 & \frac{tan(PFA_i)}{V_{g_i}} & \frac{-1}{T_{iq_i}} & 0 \\ \frac{K_{qv_i}}{T_{g_i}} & 0 & \frac{-1}{T_{g_i}} & \frac{-1}{T_{g_i}} \end{bmatrix}_{4\times4};$$

$$A_{IBR_{2i}} = A_{IBR_{3i}} = [0]_{4\times4};$$

$$A_{IBR_{4i}} = \begin{bmatrix} \frac{-1}{T_{rf_i}} & 0 & 0 & 0 \\ \frac{K_{ig}}{R_{p_{ii}}} - \frac{K_{pg_i}}{R_{p_i}T_{rf_i}} & 0 & 0 & 0 \\ 0 & \frac{1}{T_{pord_i}} & \frac{-1}{T_{pord_i}} & 0 \\ 0 & 0 & \frac{1}{T_{g_i}V_{g_i}} & \frac{-1}{T_{g_i}} \end{bmatrix}_{4\times4};$$

$$B_{IBR1} = \begin{bmatrix} B_{IBR1_1} & 0 & \dots & 0 \\ 0 & B_{IBR1_2} & \dots & 0 \\ \vdots & \vdots & \ddots & \vdots \\ 0 & 0 & \dots & B_{IBR1_{10}} \end{bmatrix}_{80\times20};$$

$$B_{IBR2} = \begin{bmatrix} B_{IBR2_1} & 0 & \dots & 0 \\ 0 & B_{IBR2_2} & \dots & 0 \\ \vdots & \vdots & \ddots & \vdots \\ 0 & 0 & \dots & B_{IBR2_{10}} \end{bmatrix}_{80\times20};$$

$$C_{IBR} = \begin{bmatrix} C_{IBR_1} & 0 & \dots & 0 \\ 0 & C_{IBR_2} & \dots & 0 \\ \vdots & \vdots & \ddots & \vdots \\ 0 & 0 & \dots & C_{IBR_{10}} \end{bmatrix}_{20\times80};$$

$$D_{IBR2} = \begin{bmatrix} D_{IBR_1} & 0 & \dots & 0 \\ 0 & D_{IBR_2} & \dots & 0 \\ \vdots & \vdots & \ddots & \vdots \\ 0 & 0 & \dots & D_{IBR_{10}} \end{bmatrix}_{20\times20}$$

$$B_{IBR1_i} = \begin{bmatrix} \frac{1}{T_{rf_i}} & 0 & 0 & 0 & 0 & 0 & 0 & 0 \\ 0 & 0 & 0 & 0 & \frac{1}{T_{rf_i}} & \frac{K_{pg_i}}{R_{p_i}T_{rf_i}} & 0 & 0 \\ 0 & \frac{1}{T_{p_i}} & 0 & 0 & 0 & 0 & 0 & 0 \end{bmatrix}^T_{3*8}$$

$$B_{IBR2_i} = \begin{bmatrix} 0 & 0 & 0 & \frac{-K_{qv_i}}{T_{g_i}} & 0 & 0 & 0 & 0 \\ 0 & 0 & 0 & 0 & 0 & \frac{-K_{ig_i}}{R_{p_i}} & 0 & 0 \\ 0 & 0 & 0 & 0 & 0 & K_{ig_i} & 0 & 0 \end{bmatrix}^T_{3\times8}$$

B. State-space model of electric truck charger

Under steady-state conditions, and assuming a unity power factor, the active power from (6) simplifies to:

$$P_{CS} = \frac{2}{3}\frac{Ri_{dc}^2}{S_d^2} + V_{dc}i_{dc} \tag{20}$$

By linearising (20) and by neglecting the second-order terms of Δi_{dc} and Δv_{dc}, one obtains:

$$\Delta P_{CS} = I_{dc_0}\Delta v_{dc} + \left(\frac{4R}{3S_d^2}I_{dc_0} + V_{dc_0}\right)\Delta i_{dc} \tag{21}$$

The state-space model of the active and reactive power consumed by equivalent truck charger can be expressed as:

$$\begin{bmatrix}\Delta P_{CS}\\ \Delta Q_{CS}\end{bmatrix} = \begin{bmatrix} I_{dc_0} & \frac{4R}{3S_d^2}I_{dc_0} + V_{dc_0} \\ 0 & 0 \end{bmatrix}\begin{bmatrix}\Delta V_{dc}\\ \Delta i_{dc}\end{bmatrix} \tag{22}$$

where, I_{dc_0} and V_{dc_0} denote the rated DC current and DC voltage, respectively.

Assume that the impact of ETCS dynamics on the AC grid is mainly determined by the DC voltage and inner current loop dynamics, as described in (3) and Fig. (3). The corresponding state-space model is given by

$$\begin{bmatrix}\Delta\dot{v}_{dc}\\ \Delta\dot{i}_{dc}\end{bmatrix} = \begin{bmatrix} -\frac{K_{iv}}{K_{pv}} & \frac{1}{C_{dc}} \\ 0 & -S_{id}\frac{K_{ii}}{K_{pi}} \end{bmatrix} - \begin{bmatrix}-1\\ 0\end{bmatrix}\Delta i_{load} \tag{23}$$

C. State-space model of the network and loads

The state-space models are given by:

$$0 = C_{DG1}\Delta X_{DG_{CS}} + D_{DG3}\Delta I_g + D_{DG4}\Delta V_g + D_{N1}\Delta V_{NET} \tag{24}$$

$$0 = C_{DG2}\Delta X_{DG_{CS}} + D_{DG5}\Delta V_g + D_{N2}\Delta V_{NET} \tag{25}$$

where $\Delta X_{DG_{CS}} = \left[\Delta X^T\ \Delta X_{cs}\right]^T$ is the state vector of DGs and of the charging station, $\Delta X_{CS} = \Delta v_{dc}$ is the state variable of the charger, and $\Delta V_{NET} = \left[\Delta\theta^T\ \Delta V^T\right]^T$ is the vector matrix formed by the voltage magnitude and angle submatrices of the network buses.

Authorized licensed use limited to: Univ Catholique de Louvain/UCL. Downloaded on November 10,2026 at 18:00:57 UTC from IEEE Xplore. Restrictions apply.

D. Complete small-signal state-space model of the AC grid integrating an electric truck charging station

The complete state-space representation of the system, illustrated in Fig. 1, is expressed as:

$$\Delta\dot{X} = A_{grid}\Delta X + B_{grid}\Delta U \tag{26}$$

where A_{grid} denotes the dynamic matrix of the considered AC grid, and B_{grid} is the input matrix. The complete form of the dynamic matrix is expressed by:

$$\left[A_{grid}\right] = \left[A_g\right] - \left[B_g\right]\left[C_g\right]^{-1}\left[D_g\right] \tag{27}$$

With $A_g = \left[A_{IBR_{CS}}\right]$; $B_g = \left[B_{IBR_1} + B_{IBR_2}\right]$; $C_g = \begin{bmatrix} C_{DG1} - D_{DG3}D_{IBR1}^{-1}C_{IBR} \\ D_{DG4}D_{IBR1}^{-1}D_{IBR2}D_{DG5}^{-1}C_{DG2} + D_{DG4}D_{DG5}^{-1}C_{DG2} \end{bmatrix}$ $D_g = \begin{bmatrix} D_{DG4}D_{IBR1}^{-1}D_{IBR2}D_{DG5}^{-1}D_{N2} \\ +D_{DG4}D_{DG5}^{-1}D_{N2} + D_{N1} \end{bmatrix}$ $A_{IBR_{CS}} = \begin{bmatrix} A_{IBR} & 0 \\ 0 & A_{CS} \end{bmatrix}_{81\times81}$; $\Delta U = \left[\Delta U_1^T \quad \Delta U_2^T \quad \Delta i_{dc}\right]_{11\times1}^T$; $C_{DG1} = \begin{bmatrix} C_{IBR} & 0 \\ 0 & 0 \end{bmatrix}_{21\times81}$ and $C_{DG2} = \begin{bmatrix} 0 & 0 \\ 0 & \Delta i_{load} \end{bmatrix}_{21\times81}$ The matrices D_{DG3} , D_{DG4}, D_{DG5}, D_{N1}, and D_{N2} are defined in [13].

IV. Results

The impact of the ETCS on small-signal stability is assessed using two scenarios—with and without the ETCS connected to the local grid—under varying load conditions. Parameter values for AC grid and truck charger are given in Table I.

TABLE I
PARAMETER VALUES FOR AC GRID AND TRUCK CHARGER.

DGs	Truck charging station
T_{rv} = 0.02 s , f_n = 50 Hz	CCS = $10 * 400$ kW, V_{dc} = 750 V
T_p = 0.002 s, T_{iq} = 0.02 s	K_{pd} = 0.1 pus, K_{id} = 10 pu
T_g = 0.02 s, T_{rf} = 0.1 s	Current controller: K_{pq} = 0.9 pu, K_{iq} = 60 pu
R_p = 20 pu, K_{qv} = 5 pu	DC voltage controller: K_{pdc} = 0.045 pu, K_{idc} = 4.8 s
K_{pg} = 0.1 pu, K_{ig} = 10 pu	LCL filter: L_{f1} = 20µF L_{f2} = 40µF, C_f = 4400µF

TABLE II
MODES CORRESPONDING TO THE CONNECTION OF 50% OF THE SUBSCRIBED LOAD POWER AT ALL BUSES ARE DEPICTED IN GREEN.

Grouped mode values	Identification of modes
$\lambda_{1_i} = -6,667$	$\Delta\theta_{PLL_i}$
$\lambda_{2_i} = -6,692$	$\Delta\theta_{PLL_i}$
$\lambda_{3_i} = -10$	Δs_{5_i}
$\lambda_{4_i} = -16,667$	$\Delta\theta_{grid_i}$
$\lambda_{5_i} = -16,667$	$\Delta\theta_{grid_i}$
λ_{6_i}, λ_{7_i}: $-18.85 \pm j6.779$	Δs_{2_i} *and* Δs_{7_i}
$\lambda_{8_i} = -47,538$	Δs_{1_i}, Δs_{3_i} *and* Δs_{4_i}
$\lambda_{9_i} = -52.5$	Δs_{4_i} (Δs_{8_i})
$\lambda_{10_i} = -100$	$\Delta grid$
λ_{11_i}, λ_{12_i}: $-54,132 \pm j7,26$	Δs_{1_i}, Δs_{3_i}, Δs_{4_i} *and* Δs_{8_i}
$\lambda_{13_i} = -62,3$	Δs_{2_i}, Δs_{6_i} *and* Δs_{7_i}

A. Scenario without an electric truck charging station connected to the local grid, under varying load conditions

Fig. 5 and Table II present the modes in the complex plane derived from the state-space model of the AC grid, defined by the configuration shown in Fig. 1, without integrating an ETCS. The results indicate that all modes are stable. Among these modes, two are associated with the voltage angle at

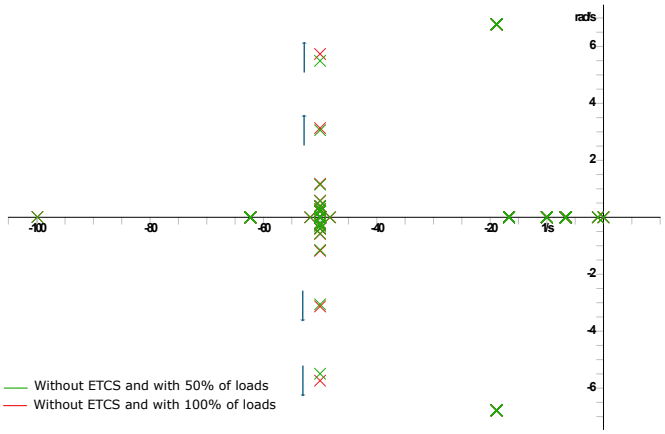


Fig. 5. The modelled system's modes in the complex plane: without connecting the ETCS to the AC grid, under varying load conditions.

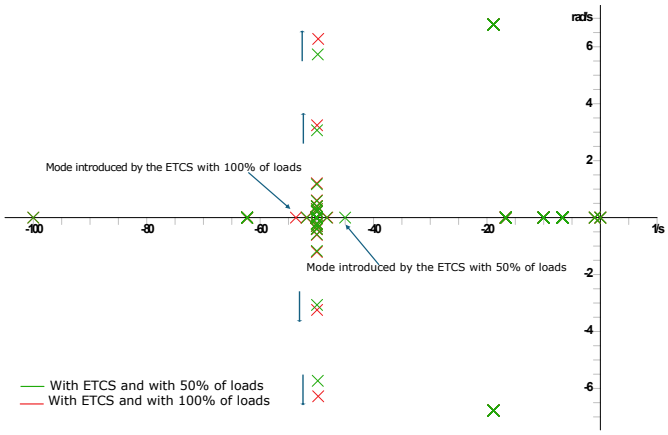


Fig. 6. The modelled system's modes in the complex plane: with connecting ETCS to the grid, under varying load conditions.

the high-voltage AC grid bus ($\Delta\theta_{grid_i}$), which is modeled as an external grid. Two additional modes are related to the voltage angle at the DG connection buses ($\Delta\theta_{PLL_i}$), while the remaining modes correspond to the DG units. Note that the dynamic behavior of the modes in the complex plane is influenced by the operating condition of the local grid, whether with 50% (green color) or 100% (red color) of the subscribed load power connected at all busses. Among the identified modes, only the complex-conjugate pairs corresponding to the state variables related to the voltage dynamics (Δs_{1_i}) and the reactive and active current-filter dynamics (Δs_{4_i} and Δs_{8_i}) exhibit pronounced sensitivity to load variations.

B. Scenario with an electric truck charging station connected to the local grid, under varying load conditions

Fig. 6 presents the results obtained by assuming that the 4MW truck charging station is connected to the local grid at the end of the half loop. Note that the equivalent truck charger model introduces an additional mode in the complex plane due to the DC voltage bus, which may affect the dynamic behavior of the local AC grid. Compared to the scenario without the charging station (Fig. 5). Its presence affects the oscillation

Authorized licensed use limited to: Univ Catholique de Louvain/UCL. Downloaded on November 10,2026 at 18:00:57 UTC from IEEE Xplore. Restrictions apply.

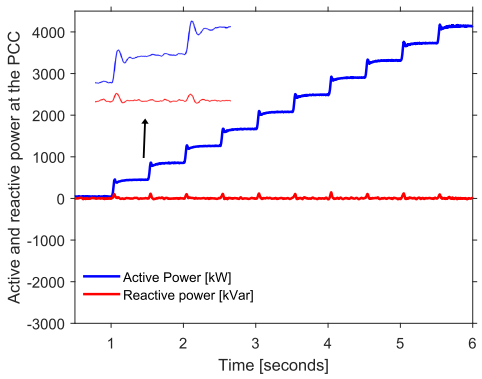


Fig. 7. Active and reactive power exchanged between public grid (PCC) and electric truck charging station.

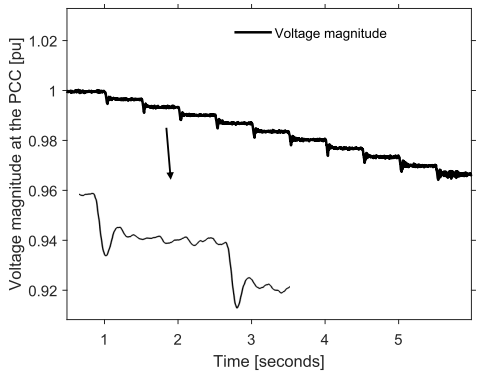


Fig. 8. Voltage profile at the PCC due to the sequential connection of trucks into charging station.

modes by increasing their frequencies. The dynamic behavior of these modes is more significantly affected under 100% conditions than under 50% conditions. The results indicate that the modes related to the voltage and current-filter dynamics (Δs_{1_i}, Δs_{4_i} and Δs_{8_i}) are the most affected by the interaction between the local grid and the ETCS. Moreover, the additional mode introduced by the charging station is more significantly affected when 100% of the subscribed load power is connected at all buses.

C. Dynamic response of the exchanged power and the voltage

The results are obtained by assuming that 50% of the subscribed load power is connected at all load buses. Fig. 7 shows the active and reactive power exchanged at the PCC during the sequential connection of trucks rated at 400 kW, occurring every 0.5 s. Note that the active power demand increases with the number of trucks connected to the charging station, whereas the reactive power is maintained at zero by the front-end rectifier control. Fig. 8 presents the voltage magnitude response at the PCC under the dynamic operation of the charging station. The rapid voltage change is estimated at 3.5%, as shown in Fig. 8. This value exceeds the mandatory threshold defined in the IEC-61000-3-7 standard.

V. Conclusion

The dynamic impact of an electric truck charging station on the small-signal stability and rapid voltage changes of the AC grid is investigated. A state-space approach is employed to assess small-signal stability by analyzing the movement of system modes in the complex plane. The obtained results show that connecting a truck charging station to the Belgian MV test grid introduces additional stable modes, whose trajectories depend on the level of subscribed load power connected to the local grid. In addition, the effects of the sequential connection of trucks on rapid voltage changes in the MV grid are investigated. The results show that the internal dynamics of the DC-microgrid-based charging station significantly influence the rapid voltage variations of the AC grid.

References

[1] X. Zhu, P. Mishra, B. Mather, M. Zhang and A. Meintz, “Grid Impact Analysis and Mitigation of En-Route Charging Stations for Heavy-Duty Electric Vehicles,” in IEEE Open Access Journal of Power and Energy, vol. 10, pp. 141-150, 2023.

[2] X. Zhu, B. Mather and P. Mishra, ”Grid Impact Analysis of Heavy-Duty Electric Vehicle Charging Stations,” 2020 IEEE Power&Energy Society Innovative Smart Grid Technologies Conference, USA, 2020, pp. 1-5.

[3] R. El Helou, S. Sivaranjani, D. Kalathil, A. Schaper, L. Xie, ”The impact of heavy-duty vehicle electrification on large power grids: A synthetic Texas case study,” Advances in Applied Energy, Vol. 6, 2022, 100093.

[4] F. Safdarian et al., ”Technical Impacts of Light-Duty and Heavy-Duty Transportation Electrification on a Coordinated Transmission and Distribution System,” in IEEE Transactions on Transportation Electrification, vol. 11, no. 1, pp. 3404-3417, Feb. 2025.

[5] A. Hassan, W. Hong, B. Wang and W. Su, “Impact of Medium and Heavy-Duty Electric Vehicle Electrification on Distribution System Stability,” 2025 IEEE ITEC+EATS, Anaheim, CA, USA, 2025, pp. 1-3.

[6] A. K. Karmaker, S. Behrens and H. Pota, “Sensitivity Analysis for Electric Vehicle Hosting Capacity in Distribution Networks,” 2023 IEEE Transportation Electrification Conference and Expo, Asia-Pacific (ITEC Asia-Pacific), Chiang Mai, Thailand, 2023, pp. 1-7.

[7] I. Nutkani, H. Toole, N. Fernando, L. P. Chiang Andrew, “Impact of EV charging on electrical distribution network and mitigating solutions – A review,” IET Smart Grid, Vol. 7, 2024, pp. 485-502.

[8] R. S. K. Moorthy, M. Starke, B. Dean, A. Adib, S. Campbell and M. Chinthavali, “Megawatt Scale Charging System Architecture,” 2022 IEEE ECCE, Detroit, MI, USA, 2022, pp. 1-8.

[9] F. Ahmed, S. Ahmad, M. Toufikur Rahman, Md. Rifat Hazari, R. Faiz, T. Ahmed, M. Karimi, “A holistic review of electric vehicle charging impacts on power distribution networks: Technical challenges, smart mitigation strategies and future directions,” Applied Energy, vol. 402, Part B, 2026, 126961.

[10] R. T. Elliott, A. Ellis, P. Pourbeik, J. J. Sanchez-Gasca, J. Senthil and J. Weber, “Generic photovoltaic system models for WECC - A status report,” 2015 IEEE Power&Energy Society General Meeting, Denver, CO, USA, 2015, pp. 1-5.

[11] C.H. Dharmakeerthi, N. Mithulananthan, T.K. Saha,“Impact of electric vehicle fast charging on power system voltage stability,” International Journal of Electrical Power&Energy Systems,Vol.57, 2014, pp.241-249.

[12] A. Arancibia and K. Strunz, “Modeling of an electric vehicle charging station for fast DC charging,” 2012 IEEE International Electric Vehicle Conference, Greenville, SC, USA, 2012, pp. 1-6

[13] G. Wanlongo Ndiwulu, E. Vasquez Mayen, and E. De Jaeger, “Effect of a Large Proton Exchange Membrane Electrolyser on Power System Small-Signal Angular Stability,” Electricity 4, no. 4; 2023,pp. 381-409.

[14] T. Oberliessen, D. Feismann, F. Klausmann, F. Otteny and C. Rehtanz, ”Simulation-Based Analysis of Grid Impact from Large-Scale HDEV Charging Infrastructure,” 2025 8th International Conference on Circuits, Systems and Simulation (ICCSS), Vietnam, 2025, pp. 99-103.

[15] M. Loupa, M. Bendle, S. Ahmed, M. Alamaniotis and N. Gatsis, ”Assessing the Impacts of Depot Charging for Medium- and Heavy-Duty Electrified Fleets on the Distribution Grid,” 2025 IEEE Texas Power and Energy Conference (TPEC), College Station, TX, USA, 2025, pp. 1-6.

Authorized licensed use limited to: Univ Catholique de Louvain/UCL. Downloaded on November 10,2026 at 18:00:57 UTC from IEEE Xplore. Restrictions apply.